Proc. Natl. Acad. Sci. USA
Vol. 93, pp. 2652–2657, April 1996
Biophysics

Swiveling-domain mechanism for enzymatic phosphotransfer between remote reaction sites

OSNAT HERZBERG*†, CELIA C. H. CHEN*, GEETA KAPADIA*, MARIELENA MCGUIRE‡, LAWRENCE J. CARROLL‡, SEONG J. NOH‡, AND DEBRA DUNAWAY-MARIANO‡

*Center for Advanced Research in Biotechnology, University of Maryland Biotechnology Institute, 9600 Gudelsky Drive, Rockville, MD 20850; and ‡Department of Chemistry and Biochemistry, University of Maryland, College Park, MD 20742

Communicated by Michael G. Rossmann, Purdue University, West Lafayette, IN, December 4, 1995 (received for review October 4, 1995)

ABSTRACT **The crystal structure of pyruvate phosphate dikinase, a histidyl multiphosphotransfer enzyme that synthesizes adenosine triphosphate, reveals a three-domain molecule in which the phosphohistidine domain is flanked by the nucleotide and the phospho*enol*pyruvate/pyruvate domains, with the two substrate binding sites ≈45 Å apart. The modes of substrate binding have been deduced by analogy to D-Ala-D-Ala ligase and to pyruvate kinase. Coupling between the two remote active sites is facilitated by two conformational states of the phosphohistidine domain. While the crystal structure represents the state of interaction with the nucleotide, the second state is achieved by swiveling around two flexible peptide linkers. This dramatic conformational transition brings the phosphocarrier residue in close proximity to phospho*enol*pyruvate/pyruvate. The swiveling-domain paradigm provides an effective mechanism for communication in complex multidomain/multiactive site proteins.**

Pyruvate, orthophosphate dikinase (PPDK; ATP:pyruvate, orthophosphate phosphotransferase, EC 2.7.9.1) catalyzes the reversible conversion of ATP, inorganic phosphate (P_i) and pyruvate to AMP, pyrophosphate and phospho*enol*pyruvate (PEP) (1). The enzyme is a large dimeric molecule (monomer molecular mass of ≈96,000 Da) that requires divalent cations for its activity. Its mechanism involves three phosphoryl group transfer reactions that are depicted in Fig. 1 (2, 3). Enzyme phosphorylation occurs on the N^{ε} atom of a histidine residue (4–6), which has been identified as His-455 in the amino acid sequence of PPDK from *Clostridium symbiosum*, the subject of this study (6). The pyrophosphoryl enzyme intermediate formed in the first step has been identified so far only in PPDK and PEP synthase, two enzymes with related function and amino acid sequence homology (7). Another protein with sequence homology to PPDK is enzyme I of the bacterial PEP:sugar phosphotransferase system (PTS). Here again, the homology is linked to functional similarity, because enzyme I is phosphorylated by PEP on a histidine residue (8).

A variety of biochemical and site-directed mutagenesis studies indicate that the ATP and pyruvate binding sites are nonoverlapping (9–13). The nucleotide partial reaction was studied separately from the pyruvate partial reaction by using isotope exchange and transient kinetic techniques (14, 15). Proteolytic cleavage with subtilisin and covalent binding of radiolabeled substrates established that the nucleotide and P_i binding sites span two N-terminal domains (25/13 kDa) (16), the PEP/pyruvate binding site is located on the C-terminal domain (35 kDa) (13, 17), and the catalytic histidine resides on an 18-kDa domain flanked by the other two.

For phosphotransfer from ATP to pyruvate, the histidine must shuttle between the two binding sites. The model of a "swinging peptide arm" that was first proposed by Wood and colleagues (1) to account for the required movement of the catalytic histidine has been further elaborated based on the above information (16). Two possibilities have been considered. The first invokes torsional angle changes of the histidine side chain. The second envisages a much more dramatic transition with the phosphohistidine domain changing its position such that it alternately interacts with the nucleotide and pyruvate. The refined crystal structure of PPDK from *C. symbiosum* reported here reveals that in fact the enzyme is exquisitely designed to utilize the second mechanism, as illustrated schematically in Fig. 1.§

EXPERIMENTAL METHODS

Protein Crystallization. PPDK from *C. symbiosum* was overexpressed in *Escherichia coli* and purified (7). Single crystals of PPDK were obtained at 30°C by vapor diffusion in hanging drops. Protein drops were equilibrated against reservoir solutions containing 50–55% saturated ammonium sulfate and 100 mM Hepes buffer (pH 7.0). The drops consisted of protein at ≈10 mg/ml, 20 mM imidazole buffer (pH 6.5), 100 mM KCl, 0.1 mM EDTA, and 1 mM 2-mercaptoethanol diluted by an equal volume of reservoir solution. The space group of the crystals is $P2_1$ with unit cell dimensions $a = 89.8$ Å; $b = 58.8$ Å; $c = 102.0$ Å; $\beta = 94.8°$. There is one monomer in the asymmetric unit and the solvent content is ≈56% by volume.

Structure Determination. X-ray diffraction data were collected on a Siemens (Iselin, NJ) area detector mounted on a three-circle goniostat, with monochromated CuKα x-ray supplied by a Rigaku (Danvers, MA) Rotaflex RU200BH rotating anode generator. Native data were collected to 2.3 Å resolution from a single crystal at room temperature. The data were processed by using the XENGEN package (18). The multiple isomorphous replacement (MIR) method was used to determine the structure at 2.8 Å resolution. Eight heavy atom derivatives provided useful information for phasing (Table 1). Diffraction data were acquired from a single crystal in each case. The computer program packages PHASES (19) and the program MLPHARE (20) were used for heavy atom parameter refinement and phase calculation. The uranyl derivative bound in a single site that was readily identified in a difference Patterson map (close to the postulated Mg^{2+} site in the PEP/pyruvate domain). This facilitated interpretation of all other heavy atom derivatives by cross-phased difference Fourier maps. In particular, there are 13 cysteines in PPDK, all of which bound mercurial derivatives. An aged crystal was soaked with ethylmercury phosphate (EMP). Some of the cysteine

The publication costs of this article were defrayed in part by page charge payment. This article must therefore be hereby marked "*advertisement*" in accordance with 18 U.S.C. §1734 solely to indicate this fact.

Abbreviations: PPDK, pyruvate phosphate dikinase; PEP, phospho*enol*pyruvate; PTS, phosphotransferase system; EMP, ethylmercury phosphate; MIR, multiple isomorphous replacement; DD-ligase, D-Ala-D-Ala ligase.

†To whom reprint requests should be addressed.

§The atomic coordinates have been deposited in the Protein Data Bank, Chemistry Department, Brookhaven National Laboratory, Upton, NY 11973 (reference 1DIK).

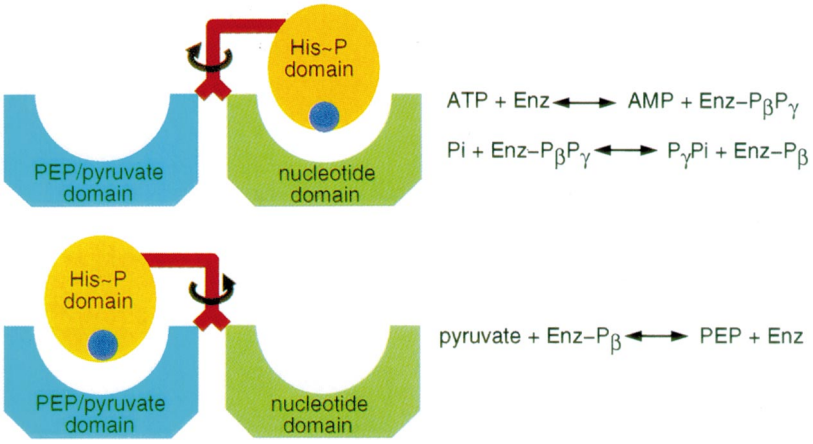

FIG. 1. A simplified model of the two conformational states of PPDK implied by the crystal structure. Partial reactions associated with each state are listed. Color scheme assigned to the domains is used throughout. Catalytic histidine is shown as a blue circle.

residues may have been oxidized in this crystal, resulting in only 7 mercury sites. Two mutant proteins were prepared. One, with a single cysteine replacement (C831A), bound EMP in 11 sites. A double cysteine replacement variant (C831A/C828A) bound EMP in 10 sites. This marked the location of the two cysteines and helped start the tracing of the polypeptide chain. Anomalous scattering data were used to establish the correct hand. Only heavy atom sites that refined with significant occupancy values in MLPHARE were included in the phase generation step using either MLPHARE or PHASES. The phase set generated by MLPHARE had a figure of merit of 0.64 and the figure of merit of the phases generated by PHASES was 0.68. The MIR phases were improved by solvent flattening techniques (21). Both the procedure of Leslie (22) and of PHASES were used. The polypeptide chain was traced while inspecting the two MIR and the two solvent-flattened maps. The molecular model was built on an INDIGO ELAN workstation using the program O (23). The structure was refined with the program X-PLOR (24) by using the simulated annealing slow-cooling protocol at 3000 K and including data between 6.0 and 2.3 Å for which $F \geq 2\sigma(F)$. Two cycles of simulated annealing alternated by adjustments to the model on the computer graphics workstation were followed by five cycles of positional refinement and model adjustments.

RESULTS AND DISCUSSION

Quality of the Structure. The current model has a conventional R factor of 0.182 for the 34,662 reflections between 8.0 and 2.3 Å resolution for which $F \geq 2\sigma(F)$ (80% of the collected data). The stereochemical parameters are well within the range known from crystal structures of small peptides. The rms deviations from ideal values for bond lengths and bond angles are 0.020 Å and 2.2°, respectively. The model includes 869 of the 874 amino acid residues (the N-terminal methionine and residues 506–509 are associated with regions of low electron density), 369 water molecules, and 3 sulfate anions.

Overall Structure. PPDK is an elongated dimer of approximate dimension of 150 × 90 × 50 Å (Fig. 2*A*). Each monomer (≈100 × 50 × 50 Å) consists of three independently folded domains (Fig. 2*B*) that correspond to the functional domains identified biochemically. The dimer interface is formed exclusively by the PEP/pyruvate binding domain and the architecture precludes the possibility of phosphotransfer across monomers. The nucleotide binding site is located ≈45 Å from the PEP/pyruvate binding site. The histidine with the phosphoryl transfer function (His-455) resides on a separate domain, which is linked to the two remote substrate binding domains by two interacting polypeptide segments (Fig. 2*B*). In this crystal form, the phosphohistidine domain is in close proximity to the nucleotide binding domain and removed from the PEP/pyruvate binding domain.

The nucleotide binding domain can be further divided into three subdomains. One (residues 2–111 and 199–249), with an $\alpha+\beta$ fold, includes a five-stranded antiparallel β-sheet. An insertion within this domain (residues 112–198) forms a four-helix bundle. The third subdomain (residues 250–340) adopts an $\alpha+\beta$ fold in which a single helix packs against a 5-stranded antiparallel β-sheet. Despite the lack of significant amino acid sequence homology, the fold of the first and third subdomains is similar to that of the nucleotide binding domains of several ATP/ADP-converting enzymes: D-Ala-D-Ala ligase [DD-ligase (25, 26)], succinyl-CoA synthetase (27), and glutathione synthase (28). Using the program ALIGN written by Cohen (29),

Table 1. Diffraction data statistics for native and heavy atom derivatives of PPDK

Data	Resolution, Å	No. of unique reflections	Completeness, %	R_{sym}	R_{iso}	Sites, no.	R_{cen}
Native	2.3	44,378	93	0.082			
0.5 mM $UO_2(NO_3)_2$ (cocrystal)	3.0	20,178	88	0.106	0.15	1	0.78
1 mM EMP (wt)	3.0	20,602	90	0.097	0.26	7	0.72
0.5 mM EMP (C831A)	3.0	21,297	93	0.110	0.33	11	0.67
0.5 mM EMP (C828A/C831A)	3.2	16,348	89	0.097	0.26	10	0.75
0.5 mM PCMBS (C831A)	2.9	23,080	91	0.083	0.14	2	0.85 (3Å)
1 mM Na mersalyl (wt)	3.1	19,202	97	0.084	0.17	5	0.79
1 mM $LuCl_3$ (wt)	3.0	18,275	80	0.080	0.13	3	0.86
1 mM $SmCl_3$ (wt)	3.3	16,118	98	0.105	0.20	3	0.82 (5Å)

PCMBS, *p*-chloromercuribenzenesulfonate; wt, wild type. $R_{sym} = \Sigma_h\Sigma_i|<I(h)>-I(h)_i|/\Sigma_h\Sigma_i I(h)_i$ for symmetry-related observations. $R_{iso} = \Sigma_h(||F_{PH}|-|F_P||)/\Sigma_h|F_P|$. $R_{cen} = \Sigma_h||F_P+F_H(\text{calc})|-|F_{PH}||/\Sigma_h||F_{PH}|-|F_P||$ for centric reflections (values from MLPHARE).

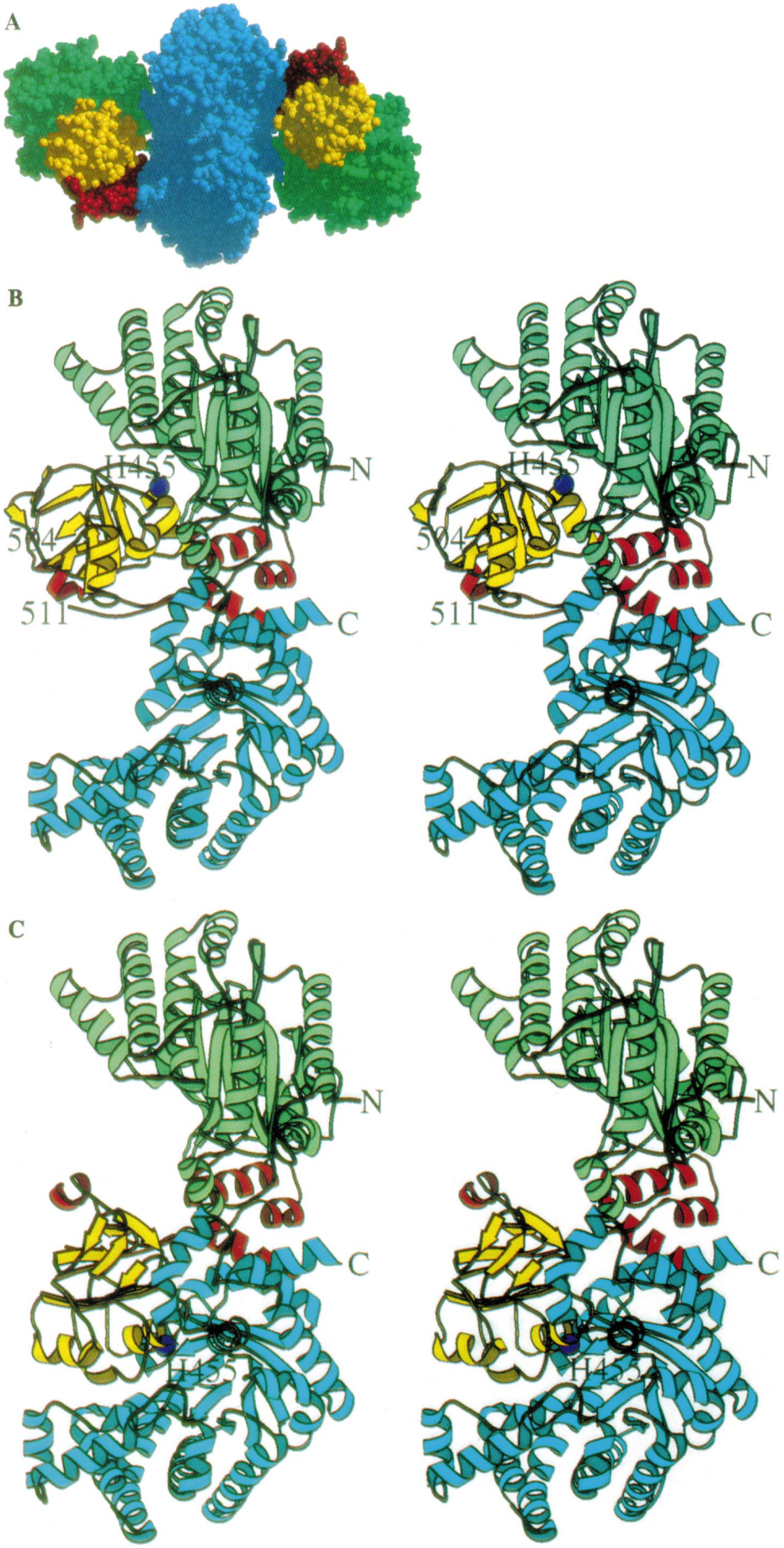

FIG. 2. Overall PPDK molecule, highlighting its structural domains in different colors: green, nucleotide binding domain; gold, phosphohistidine domain; blue, PEP/pyruvate binding domain; red, linker peptides. (*A*) Space filling model of the dimer associated around the crystallographic twofold axis. (*B*) Ribbon diagram of the monomer; position of His-455 is shown as a blue sphere. Discontinuity in the polypeptide chain observed in the crystal between residues 504 and 511 is marked. (*C*) Ribbon diagram of a model of the second conformational state of PPDK in which the phosphohistidine domain interacts with the PEP/pyruvate domain. It has been obtained by a swivel motion of ≈100° around residue 380.

the α-carbon atoms of the nucleotide binding domain of PPDK were superimposed on the nucleotide binding domains of the above enzymes. The rms deviations are 2.2 Å for 155 residue pairs, 2.4 Å (155 residues), and 2.4 Å (126 residues), respectively.

The phosphohistidine domain spans residues 390–504 and consists of a scaffold of $\beta/\beta/\alpha$ layers with two 4-stranded orthogonal β-sheets. One is antiparallel and the second is parallel and covered by three helices. The two β-sheets are somewhat splayed apart to accommodate a third 3-stranded antiparallel β-sheet. A related three-layer $\beta/\beta/\alpha$ architecture has been proposed as a folding class in SCOP (30) and so far includes one member, aconitase (31), which only remotely resembles the fold of the phosphohistidine domain.

The third domain, the PEP/pyruvate binding domain spanning residues 534–874, forms an 8-stranded α/β-barrel. The pyruvate binding domain of pyruvate kinase also forms an α/β barrel (32), albeit with no significant amino acid sequence homology with PPDK. Comparison of the α/β barrel of PPDK with other barrels in the Brookhaven Protein Data Bank using the program DALI (33) reveals that the barrel of pyruvate kinase is structurally the most similar to that of PPDK. The α-carbon atoms of the two structures have been superpositioned with a rms deviation of 2.1 Å for 192 residue pairs.

Two polypeptide segments connect the phosphohistidine domain to the nucleotide and PEP/pyruvate binding domains (residues 341–389 and 504–533 highlighted in red in Fig. 2). They are partly helical and interact with each other. Segments closest to the start and end of the phosphohistidine domain have high crystallographic temperature factors, and four residues (residues 506–509) are completely disordered in the current model. This local conformational flexibility may be important during phosphotransfer.

Substrate Binding Sites. The location and approximate mode of nucleotide and Mg^{2+} binding may be deduced by analogy with the DD-ligase structure that has been determined in the presence of Mg^{2+}/ADP and a phosphinophosphate inhibitor (25), and the Mg^{2+}/PEP/pyruvate binding mode may be deduced by analogy with the pyruvate kinase structure determined in the presence of Mn^{2+}/pyruvate (32). The superpositions of these two structures on the respective domains of PPDK highlight the invariant common features that facilitate substrate binding.

Similarly to pyruvate kinase, either PEP or pyruvate can be accommodated close to the center of the α/β-barrel, at the C-terminal end of the β-strands (Fig. 3*A*). Clusters of negatively and positively charged residues provide the electrostatic environment to counter the carboxyl and the phosphoryl groups of the modeled PEP and Mg^{2+}. Small adjustments to the conformation of three side chains have been made to avoid van der Waals clashes and to facilitate favorable interactions between Arg-561, Arg-617, and the phosphoryl group of PEP, and between Asp-769 and Glu-745 and the magnesium cation. The carboxylate moiety of the modeled pyruvate interacts with the N terminus of a short helix, as seen in pyruvate kinase. The residues that interact with Mg^{2+}, Asp-769 and Glu-745, are invariant in PPDK, pyruvate kinase, PEP synthase, and enzyme I. The phosphoryl group in the model is facing the solvent, poised for an in-line transfer to His-455. Interestingly, Arg-617 is located in an equivalent position to that of the K^+ in pyruvate kinase, which lacks an arginine pair. Thus, if monocations play a role in PPDK activity, it is not expected to be the same as in pyruvate kinase.

The methylene group of the pyruvate moiety is located close to Cys-831, although the thiol group, seen in the crystal at the apo state, is oriented away from the methylene group. The mutant enzyme C831A, originally prepared for the heavy atom derivative work, cannot accept a phosphoryl group from PEP (34). The C831A crystal is isomorphous with that of the wild-type enzyme, indicating that the fold is intact. Therefore, Cys-831 must play a catalytic role, most likely by providing the proton to the enolate form of pyruvate. In contrast to pyruvate

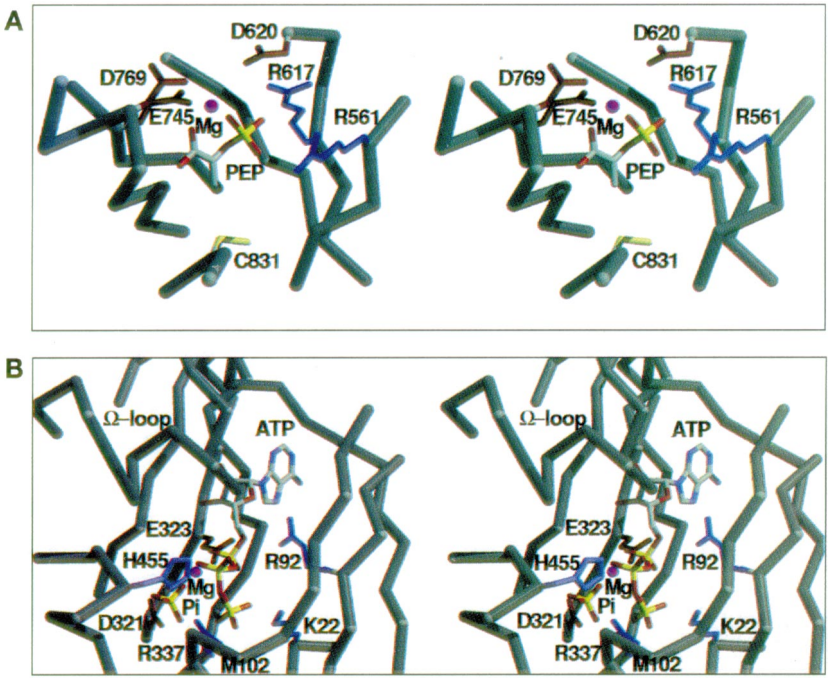

FIG. 3. Stereoscopic views of modeled substrates in their respective binding sites. Virtual bonds between α-carbon atoms are gray. Shapely colors are used for protein side chains: blue, positively charged residues; red, negatively charged residue; yellow, cysteine. Substrate molecules are shown in CPK atomic colors. Mg^{2+} is magenta. (*A*) Mg^{2+}/PEP in the PEP/pyruvate binding site. Conformations of the side chains of Arg-561, Arg-617, and Asp-769 have been adjusted to obtain favorable electrostatic interactions with the modeled PEP. No change has been made to the side chain of Cys-831. (*B*) Mg^{2+}/ATP and P_i in the nucleotide binding site. Conformation of His-455 has been adjusted for in-line attack on the β-phosphate of ATP. The Ω-loop that blocks nucleotide access is marked. The γ-phosphate of ATP is located in the oxyanion hole and P_i is in an equivalent position to that of the phosphate group of the phosphinophosphate inhibitor in the DD-ligase structure.

kinase, where the structural information cannot distinguish between the proton acceptor/donor role being played by Thr-327 or by Lys-269 (32), in PPDK Cys-831 is the only candidate. The cysteine occupies a similar position to Thr-327 in pyruvate kinase, and instead of Lys-269 there is a methionine in PPDK (Met-743).

While the PEP/pyruvate binding site is accessible to the substrate in this crystal form, the nucleotide binding site of PPDK is partially blocked compared with that of the DD-ligase. A main-chain conformational transition of an Ω-loop (residues 273–288) is required so that residues 278–280 are removed from a site that should be occupied by the ribose moiety (Fig. 3*B*). The loop conformation is expected to be different from that of the corresponding loop in the DD-ligase (residues 205–221), which carries a lysine residue (Lys-215) that interacts with the β-phosphate group of the ADP. This is impossible in PPDK because it is the catalytic His-455 that should occupy the equivalent position. A view of the actual loop conformation in the bound state awaits further crystallographic studies.

In the current crystal form, the phosphohistidine domain interacts closely with the nucleotide binding domain and the side chain of His-455 adopts a conformation such that its N^{ε} atom is buried. However, modeling shows that a conformation accessible to phosphorylation is easily achieved by a rotation around the C^{α}-C^{β} bond. With the exception of this modification, adopted for in-line attack on the β-phosphate group of ATP, no other adjustments have been made.

The nucleotide active site depression is lined with several charged amino acid residues, which should form favorable electrostatic interaction with Mg^{2+}/ATP (Lys-22, Arg-92, Arg-337, Asp-321, Glu-323). Moreover, a sulfate ion (Fig. 4) is tightly bound in a site that is occupied by the γ-phosphate of the modeled ATP. An anionic moiety at this site forms favorable electrostatic interactions with Arg-337 and Lys-22 and with an oxyanion hole comprising the amide groups of Gly-101 and Met-103. The model in Fig. 3*B* shows the P_i interacting with Arg-337 and the Mg^{2+}, and in close proximity to the γ-phosphate. An alternative arrangement in which the positions of the P_i and the γ-phosphate group of ATP are swapped is also sterically and functionally possible. With either arrangement, the crystal structure indicates that the nucleotide and the P_i share the same active site, thus two of the three partial catalytic steps occur in the context of this domain.

Mechanism for Communication Between the Remote Active Sites. The nucleotide and PEP/pyruvate binding sites in PPDK are located some 45 Å apart and clearly could not communicate without the phosphohistidine domain playing a go-between role. Each of the substrate binding sites is located in a depression, whereas His-455 is located on a convex surface of the phosphohistidine domain that can complement concave surfaces. Modeling reveals that shuttling His-455~P between the two active sites must involve a dramatic swivel of the phosphohistidine domain so that the histidine is always facing one of the bound substrates for productive phosphoryl group transfer to occur (Fig. 1). The conformational state corresponding to the interaction between the phosphohistidine domain and the PEP/pyruvate domain has been modeled (Fig. 2*C*). Consistent with other biological phosphotransfer reactions (35), and similar to the approach taken to model phosphotransfer between the PTS proteins HPr (heat-stable protein) and IIA (36), an associative pathway has been assumed, with a transition state of pentagonally coordinated phosphorous in trigonal bipyramidal geometry and the donor and acceptor groups at apical positions. Complementary surfaces of the phosphohistidine and the PEP/pyruvate domains are obtained by pivoting around the extended polypeptide segments of the linker regions while maintaining main-chain dihedral angle values that are commonly observed in known structures. The phosphohistidine domain is accommodated without major clashes. The conformational transition exposes ≈700 $Å^2$ of the molecular surface of the nucleotide binding domain (calculated using QUANTA). Eighteen amino acid residues that contact the phosphohistidine domain (4.5 Å cutoff criteria) become exposed to solvent. Five of these form interdomain electrostatic interactions (3.5 Å cutoff criteria) in the crystallographically observed structure. On the other hand, new interactions are formed between the pyruvate/PEP binding domain and the phosphohistidine domain. This should be considered an approximate model that demonstrates the type of domain movement that is likely to occur. An accurate evaluation of the conformational space sampled by the linker regions and of the alternative interdomain contacts awaits the crystal structure determination of this second structural state.

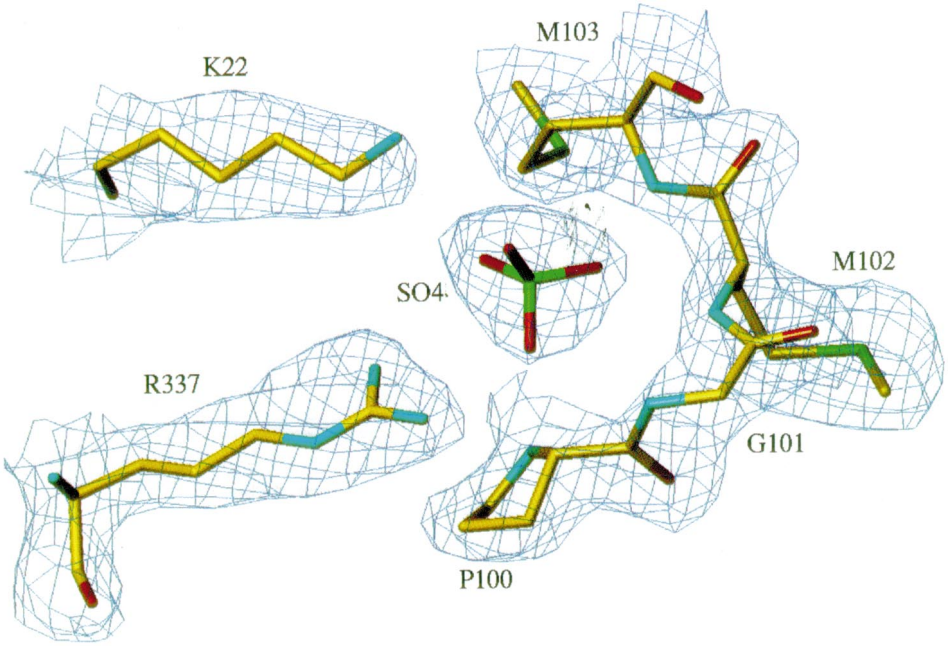

FIG. 4. View of the region of the electron density map in the vicinity of the sulfate ion at the nucleotide binding site. The 2.3-Å-resolution map with the coefficients $2F_o - F_c$ and calculated phases is displayed together with the refined model.

Because of the functional and sequence homology, a similar mechanism of phosphotransfer linked to swiveling-domain movements is expected to take place in PEP synthase and between the bacterial PTS protein pair enzyme I and HPr.

What is the driving force for this long-range conformational transition? One could speculate about two mechanistic models that are not necessarily mutually exclusive: First, the crystal structure shows that there are ample charge–charge interactions within the active sites, within the domain, and between domains; thus switching between alternative arrangements of charge–charge interactions driven by electrostatic changes due to phosphorylation may lead to the conformational transition. Because the charge distribution of this large molecule is so complex, analysis of a possible chain of events requires knowledge of the exact electrostatic interactions in both states. Second, the apparent structural independence of the two linker units, together with the ease of accommodation of the phosphohistidine domain in the depressions of either active sites, indicates that the reaction may be kinetically controlled. The phosphohistidine domain could constantly swivel, and the outcome depends on the availability of substrates. Evidence for such a mechanism may be obtained by engineering more or less flexibility into the linker regions by site-directed mutagenesis.

The mode of domain communication revealed by the crystal structure of PPDK can be contrasted with the mechanism of coupling two partial reactions catalyzed by tryptophan synthetase (37). With two active sites located on separate subunits, the product of the first reaction diffuses through an internal tunnel shielded from solvent to arrive at the second reaction site. PPDK utilizes a very different mechanism in which the substrates/products are remote and static, and a dynamic protein domain facilitates catalysis. This may turn out to be a general mode of communication used by many other multidomain enzymes.

We acknowledge Liisa Holm and Chris Sander who first identified the similarity in fold between PPDK and glutathione synthase. We are thankful to John Moult for his insightful discussions. We thank Jim Knox, Hazel Holden, and Ivan Rayment for providing coordinates prior to their public release and Linda Yankie, Yuan Xu, and Sara Thrall for help with protein preparation. This work was supported by National Science Foundation Grant MCB9316934 (O.H.), National Science Foundation Research Planning Award DMB9109951 (C.C.H.C.), and National Institutes of Health Grant GM36260 (D.D.-M.).

1. Wood, H. G., Obrien, W. E. & Michaels, G. (1977) *Adv. Enzymol.* **45,** 85–155.
2. Evans, H. J. & Wood, H. G. (1968) *Proc. Natl. Acad. Sci. USA* **61,** 1448–1453.
3. Cook, A. G. & Knowles, J. R. (1985) *Biochemistry* **24,** 51–58.
4. Spronk, A. M., Yoshida, H. & Wood, H. G. (1976) *Proc. Natl. Acad. Sci. USA* **73,** 4415–4419.
5. Milner, Y., Michaels, G. & Wood, H. G. (1978) *J. Biol. Chem.* **253,** 878–883.
6. Goss, N. H., Evans, C. T. & Wood, H. G. (1980) *Biochemistry* **19,** 5805–5809.
7. Pocalyko, D. J., Carroll, L. J., Martin, B. M., Babbitt, P. C. & Dunaway-Mariano, D. (1990) *Biochemistry* **29,** 10757–10765.
8. Weigel, N. M. A., Kukurunzunska, M. A., Nakazawa, A., Waygood, E. B. & Roseman, S. (1982) *J. Biol. Chem.* **257,** 14477–14491.
9. Yoshida, H. & Wood, H. G. (1978) *J. Biol. Chem.* **253,** 7650–7655.
10. Evans, C. T., Goss, N. H. & Wood, H. G. (1980) *Biochemistry* **19,** 5809–5814.
11. Jenkins, C. L. D. & Hatch, M. D. (1985) *Arch. Biochem. Biophys.* **239,** 53–62.
12. Thrall, S. H. & Dunaway-Mariano, D. (1994) *Biochemistry* **33,** 1103–1107.
13. Xu, Y., McGurie, M., Dunaway-Mariano, D. & Martin, B. M. (1995) *Biochemistry* **34,** 2195–2202.
14. Wang, H. C., Ciskanik, L., Dunaway-Mariano, D., von der Saal, W. & Vilafranca, J. J. (1988) *Biochemistry* **27,** 625–633.
15. Mehl, L. J., Carroll, L. J. & Dunaway-Mariano, D. (1994) *Biochemistry* **33,** 1093–1102.
16. Carrol, L. J., Xu, Y., Thrall, S. H., Martin, B. & Dunaway-Mariano, D. (1994) *Biochemistry* **33,** 1134–1142.
17. Yankie, L., Xu, Y. & Dunaway-Mariano, D. (1995) *Biochemistry* **34,** 2188–2194.
18. Howard, A. J., Gilliland, G. L., Finzel, B. C., Poulos, T., Ohlendorf, D. O. & Salemme, F. R. (1987) *J. Appl. Crystallogr.* **20,** 383–387.
19. Furey, W. & Swaminathan, S. (1990) *Program and Abstract Book: 1990 Annual Meeting* (Am. Crystallogr. Assoc., Buffalo, NY), abstr. PA33.
20. Otwinowski, Z. (1991) in *Isomorphous Replacement and Anomalous Scattering*, eds. Wolf, W., Evans, P. R. & Leslie, A.G.W. (SERC Daresbury Lab., Warrington, U.K.), pp. 80–86.
21. Wang, B. C. (1985) *Methods Enzymol.* **115B,** 90–112.
22. Leslie, A. G. W. (1987) *Acta Crystallogr. A* **43,** 134–136.
23. Jones, T. A., Zou, J.-Y., Cowan, S. W. & Kjeldgaard, M. (1991) *Acta Crystallogr. A* **47,** 110–119.
24. Brünger, A. T., Kuriyan, J. & Karplus, M. (1987) *Science* **235,** 458–460.
25. Fan, C., Moews, P. C., Walsh, C. T. & Konx, J. R. (1994) *Science* **266,** 439–443.
26. Fan, C., Moews, P. C., Shi, Y., Walsh, C. T. & Knox, J. R. (1995) *Proc. Natl. Acad. Sci. USA* **92,** 1172–1176.
27. Wolodko, W. T., Fraser, M. E., James, M. N. G. & Bridger, W. A. (1994) *J. Biol. Chem.* **269,** 10883–10890.
28. Yamaguchi, H., Koto, H., Hata, Y., Nishioka, T., Kimara, A., Oda, J. & Katsube, Y. (1993) *J. Mol. Biol.* **229,** 1083–1100.
29. Satow, Y., Cohen, G. H., Padlan, E. A. & Davies, D. R. (1986) *J. Mol. Biol.* **190,** 593–604.
30. Murzin, A. G., Brenner, S. E., Hubbard, T. & Chothia, C. (1995) *J. Mol. Biol.* **247,** 536–540.
31. Robbins, A. H. & Stout, C. D. (1989) *Proc. Natl. Acad. Sci. USA* **86,** 3639–3643.
32. Larsen, T. M., Laughlin, L. T., Holden, H. M. & Rayment, I. (1994) *Biochemistry* **33,** 6301–6309.
33. Holm, L. & Sander, C. (1993) *J. Mol. Biol.* **233,** 123–138.
34. Xu, Y., Yankie, L., Seng, L., Jung, Y-S., Mariano, P. & Dunaway-Mariano, D. (1995) *Biochemistry* **34,** 2181–2187.
35. Knowles, J. R. (1980) *Annu. Rev. Biochem.* **49,** 877–919.
36. Herzberg, O. (1992) *J. Biol. Chem.* **267,** 24819–24823.
37. Hyde, C. C., Ahmed, S. A., Padlan, E. A., Miles, E. W. & Davis, D. R. (1988) *J. Biol. Chem.* **263,** 17857–17871.